Pyrolysis-Induced Fragmentation and Blowoff of Laser-Irradiated Surfaces

Girard A. Simons*
Physical Sciences Inc., Andover, Massachusetts

During pyrolysis of a laser-irradiated material, large pressures must develop within the internal porous structure in order to transport the volatile gases to the free surface. These high internal pressures may cause macroscopic fracture and/or solid-phase mass removal prior to complete pyrolysis or vaporization. A pyrolysis/volatile transport model is used to assess the conditions under which this enhanced mass removal mechanism will occur. Critical energy densities (≈kJ/g) are predicted to be relatively insensitive to the physical parameters involved. The threshold pulse fluence (J/cm^2 absorbed by the target) is sensitive to the laser pulse duration, the pyrolysis rate, and the laser absorption depth.

Nomenclature

a = radius of porous particle
A = pre-exponential factor of k
B = activation energy of k
B_0 = $B/2+N$
c = specific heat of target material
F = pulse fluence absorbed by target, J/cm^2
F_{th} = threshold pulse fluence for fragmentation
F_{thm} = minimum threshold pulse fluence
$\bar{g}$ = pore distribution function per sample area
k = intrinsic pyrolysis rate
K_0 = const ≈ ratio of pore length to diamater ≈5
ℓ = depth of thermal layer
ℓ_v = laser absorption depth
ℓ_p = length of pore of radius r_p
ℓ_t = length of the pore that represents the trunk of a tree
M = pre-exponential factor for δ_{max}
N = decay constant for δ_{max}
$n(y)$ = number of pores of radius r_p at location y in pore tree
p_G = gas pressure at (r_p, r_t)
p_{limit} = upper limit of p_G in the pore
p_{max} = value of p_G at (r_{min}, r_t)
p_{ref} = reference pressure, see Sec. III
r_p = radius of pore
r_{min} = radius of smallest pore
r_{max} = radius of largest pore
r_t = radius of the pore that represents the trunk of a tree
r_{jV} = radius of pore for which $\bar{u}(r_p, r_t)=0$
R = gas constant
s_p = specific internal surface area (area/mass)
t = time
T = temperature
$\bar{u}$ = bulk velocity of volatiles
$\bar{V}$ = mean thermal speed of a molecule
x = coordinate normal to free surface
x_0 = reference length, see Sec. V
x_f = location of fracture
y = skewed coordinate in pore tree
β = $\ell n(r_{max}/r_{min})$
θ = porosity
θ_f = final porosity after pryolysis
κ = thermal diffusivity
μ_G = gas viscosity
ρ_G = gas density
ρ_s = density of nonporous material
δ_{max} = material yield stress
τ_p = laser pulse duration

Received Nov. 18, 1985; revision received March 8, 1986.

*Principal Research Scientist.

I. Introduction

PYROLYSIS, pore evolution, and volatile transport within a porous media have been studied extensively in the coal pyrolysis literature.[1-4] The relatively rapid pyrolysis rates, coupled with the large internal resistance to fluid transport, induce high internal gas pressures that are potentially capable of causing fragmentation. This mechanism is responsible for enhanced mass removal from charring ablators in re-entry[5] and is examined here for its potential in enhancing the mass removal from a laser-irradiated surface.

The gas within the porous structure may reach a limiting value (p_{limit}) corresponding to a static gas at a temperature of 3000–4000 K and a gas density equal to the solid density of the material which is pyrolyzing (1 g/cm^3). This pressure is of the order of a gigapascal, i.e., $p_{limit} \simeq 1$ GPa, and, if the entire pore volume contains gas at this pressure, fragmentation is imminent. However, the permeability of the porous media may be sufficiently large, or the pyrolysis rate may be sufficiently low, that p_{limit} is not attained anywhere within the porous media. Clearly, a pore evolution/volatile transport model is required to assess the gas pressure within the porous media as a function of the pyrolysis rate, pore size, etc.

Volatile transport models[1-4] have been developed using both the random pore model[6-9] and the pore tree model[10-12] of pore structure. These two models represent extreme limits on the assumptions of pore interconnectivity and the permeability of the porous system, the pore tree offering much more resistance to fluid flow than the random pore model. The random pore model assumes that all pores intersect and mix simultaneously. Specifically, the random pore model requires that each small pore connect two larger pores.[13] This requires that the pore aspect ratio (length to diameter) be of order 100. The pore tree theory predicts that all pores possess an aspect ratio of order 10. Hence, small pores may connect to larger pores only on one end and all pores must branch from successively larger pores like a tree or river system. Key aspects of the pore tree theory, with respect to pore interconnectivity, have been validated for coal and char.[14] When applied to coal pyrolysis,[1,2] the internal pressures predicted by the pore tree theory are much greater than those predicted by the random pore model. Hence, application of the pore tree theory to pyrolysis-

induced fragmentation of laser-irradiated surfaces must be restricted to target materials whose pore structures are similar to that of coal and char; otherwise, the internal gas pressure and the tendency to fragment will be overestimated.

In order to develop a pore structure similar to that of coal char, a material must posses pyrolyzing and nonpyrolyzing components that are represented by the volatiles and the char, respectively. The pyrolyzing component must be a complex hydrocarbon, with a wide range of bond energies such that a wide range of pore sizes results from pyrolysis.[1] Composite materials consisting of fibers and resins meet these restrictions. The fibers can consist of a glass or a carbon, while the resin must be an organic compound such as an epoxy or phenolic material that will "char" in a manner similar to coal.

Recognizing that this analysis may overestimate the potential for fragmentation of noncharring materials, the pore structure model is summarized in Sec. II, the volatile transport model is described in Sec. III, and the fragmentation model is developed in Sec. IV. The model predictions are obtained in Sec. V. It is shown that: 1) the critical energy densities and pulse fluences required for fragmentation are relatively insensitive to the physical parameters involved, and 2) there is an optimum laser pulse duration, energy absorption depth, and pyrolysis rate that minimize the pulse fluence required for mechanical mass removal.

II. Pore Structure

A statistical model describing the structure of porous coal and char has been previously reported by Simons and Finson[10] and Simons.[11,12] A spherical char particle of radius a contains pores of length ℓ_p and radius r_p. While the particle size a will be replaced with the fracture depth x_f in the present application, the pore dimensions within the particle fragment will range from a microscale (on the order of nanometers) to a macroscale that is a significant fraction of the particle size. The radius of the largest pore is denoted by $r_{\max}$ and is given by

$$r_{\max} = 2\theta^{1/3} a/3K_0 \tag{1}$$

where θ is the total porosity of the char, K_0 a constant of integration relating the pore length to its radius,

$$\ell_p = K_0 r_p/\theta^{1/3} \tag{2}$$

and available data[10,14] for $r_{\max}/a$ have been used to infer $K_0 \approx 5$. The radius of the smallest pore is denoted by $r_{\min}$ and is given by

$$r_{\min} = 2\theta/\beta\rho_s s_p \tag{3}$$

where $\beta = \ell n(r_{\max}/r_{\min})$, ρ_s is the solid density of the pyrolyzed material, and s_p is the specific internal surface area (typically several hundred square meters/gram for coal and char).

The porous sample contains a continuous distribution of pore sizes from $r_{\min}$ to $r_{\max}$. The number of pores within an arbitrary cross section of area A and with radius between r_p and $r_p + dr_p$ is denoted by $\bar{g}(r_p)A dr_p$. The pore distribution function $\bar{g}(r_p)$ is given by

$$\bar{g}(r_p) = \theta/2\pi\beta r_p^3$$

where $\bar{g}(r_p)$ indicates an average over all inclination angles between the axis of the pore and the normal to the plane. Due to the random orientation of the pores, the intersection of a circular cylinder with a plane is an ellipse of average area $2\pi r_p^2$. Hence, the porosity is the $2\pi r_p^2$ moment of $\bar{g}(r_p)$ and the internal surface area is the $4\pi r_p$ moment of $\bar{g}(r_p)$. The expression for $\bar{g}(r_p)$ was derived from statistical arguments[10] and predicts that the pore volume between $r_{\min}$ and r_p increases linearly with the natural log of r_p. It is the functional form of this relationship,

$$\int_{r_{\min}}^{r_p} r_p^2 \bar{g}(r_p) dr_p = \text{const} \times \ell n r_p$$

that depicts the inverse cubic dependence of $\bar{g}(r_p)$ on r_p. A linear display of the mercury intrusion volume[14] always infers a Q/r_p^3 distribution, where Q is specified by the pore volume and is proportional to the slope of the intrusion volume with respect to $\ell n(r_p)$. Local variations in Q may be rationalized as local errors in the pore radius, which is considerably more accurate than resorting to a bi- or trimodal distribution function incorporating all the pore volume into two or three distinct pore sizes.

Each pore that reaches the exterior surface of the porous particle is depicted as the trunk of a tree. The size distribution of tree trunks on the exterior surface of the particle is denoted by $\bar{g}(r_t)4\pi a^2 dr_t$, where $\bar{g}(r_t)$ is functionally identical to $\bar{g}(r_p)$. Each trunk of radius r_t is associated with a specific tree-like structure. A detailed description of the branching sequence in the pore tree has been developed.[12] The pores branch in a continuous downsizing manner. The number $n(y)$ pores of radius r_p at position y in the pore tree is given by

$$n(y) = r_t^2/r_p^2(y) \tag{4}$$

and the coordinate y is related to r_p by

$$\frac{dr_p}{dy} = \frac{r_p}{\ell_t} \tag{5}$$

where y is positive out of the pore tree.

The branching sequence of the pore tree is a critical function[12] of the Q/r_p^3 distribution function discussed above. Hence, it is necessary to validate this distribution function (with mercury intrusion[14]) for any materials pyrolyzed by laser irradiation. Indeed, this distribution function is well validated for coal and char,[10,14] porous sorbents such as calcine,[15] and shortite[16] that are used for absorption of trace species in coal gas cleanup and even for kidney stones.[17] However, empirical validation of the pore size distribution function is always an a priori requirement for the validation of the pore tree/transport model.

The current description of the pore tree provides a realistic pore structure in which pore evolution[1] and species transport[2] during pyrolysis have been described. The transport theory provides a quantitative prediction of the gas pressure in any pore in any tree of the structure. This pressure distribution is used to assess the fragmentation due to internal pressures induced during pyrolysis of a laser-irradiated surface.

III. Transport Model

A schematic of the pore tree is illustrated in Fig. 1. The mean velocity of the volatiles $\bar{u}$ and the skewed coordinate y are positive out of the tree. At each location y, there are n pores of radius r_p within a given pore tree of trunk radius r_t. The pore growth during pyrolysis is given by[1]

$$\frac{dr_p}{dt} = \frac{r_p}{3\theta}\frac{d\theta}{dt} \tag{6}$$

or

$$r_p = r_p(o)\left(\frac{\theta}{\theta(o)}\right)^{1/3} \tag{7}$$

Equations (2) and (7) depict that the pore length is constant during pyrolysis. Pores are connected end to end in the pore tree and only the radius increases during pyrolysis.

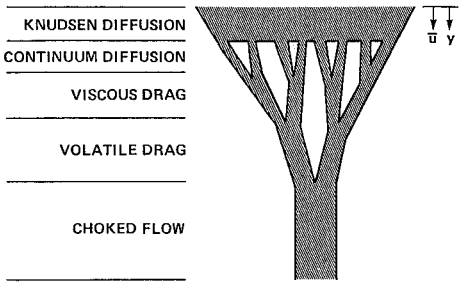

Fig. 1 Volatile flux through the pore tree.

The flux of volatiles from the wall of the pore is added to the flux through the pore tree. The continuity equation is written as[2]

$$\frac{\mathrm{d}(\rho_G \bar{u})}{\mathrm{d}r_p} = \frac{\rho_s \ell_t k(\theta_f - \theta)}{\theta r_p} \tag{8}$$

where the bulk pyrolysis rate k is defined as

$$\frac{\mathrm{d}\theta}{\mathrm{d}t} = k(\theta_f - \theta)$$

and θ_f is the final porosity after pyrolysis. Integration of Eq. (8) subject to $\rho_G \bar{u} = 0$ at $y = 0$ yields

$$\bar{u} = \frac{k\ell_t p_{\mathrm{ref}}}{p_G} \ell n\left(\frac{r_p}{r_{\min}}\right) \tag{9}$$

where

$$p_{\mathrm{ref}} = \frac{\rho_s \bar{V}^2 \pi(\theta_f - \theta)}{8\theta}$$

and $\bar{V}$ is the mean thermal speed of a molecule,

$$\bar{V} = (8RT/\pi)^{1/2}$$

When the internal pressures become significant enough to induce fragmentation, the volatile transport is limited by viscous convection.[2] The velocity and pressure are related by

$$\bar{u} = -\frac{r_p^2}{8\mu_G}\frac{\mathrm{d}p_G}{\mathrm{d}y} \tag{10}$$

Equations (9), (10), and (5) can be combined into a single differential equation for $\mathrm{d}p_G/\mathrm{d}r_p$ as a function of r_p. Integration yields

$$p_G = \frac{2\ell_t}{r_p}(k\mu_G p_{\mathrm{ref}})^{1/2}\left[2\ell n\left(\frac{r_p}{r_{\min}}\right) + 1\right]^{1/2} \tag{11}$$

for $r_p \ll r_t$. The failure equation (11) in the limit of $r_p \to r_t$ is not relevant in describing the fracture mechanics. The large pressure in the small pores is dominant in inducing fragmentation.

Equation (11) predicts that the internal pressure increases with increasing tree size and decreasing pore size. There is clearly an upper limit (p_{limit}) for the gas pressure corresponding to the situation where the solid pyrolyzes and the gas remains in the pore. This limit corresponds to a gas of density 1 g/cm^3 that, at 3000 K, generates a pressure of approximately 1 GPa.

If the pressure anywhere in the pore tree exceeds p_{limit}, Eq. (11) must be modified[2] to allow $p_G \to p_{\mathrm{limit}}$ at $r_p = r_{jV}$, where $r_{jV} > r_{\min}$. The flow velocity and pressure gradient are zero for all $r_p \le r_{jV}$ and the solution for the pressure in pores of radius greater than r_{jV} becomes

$$p_G(r_p, r_t) = p_{\mathrm{limit}}\left(\frac{r_{jV}}{r_p}\right)\left[2\ell n\left(\frac{r_p}{r_{jv}}\right) + 1\right]^{1/2} \tag{12}$$

where

$$r_{jV}(r_t) = \frac{2\ell_t}{p_{\mathrm{limit}}}(k\mu_G p_{\mathrm{ref}})^{1/2} \tag{13}$$

The above solutions for the internal gas pressure are implemented into a fracture criterion in the following section.

IV. Fragmentation Model

Macroscopic properties of a porous sample, such as fragmentation during pyrolysis, are a consequence of the integral of various pore properties over every pore in every pore tree in the porous sample. Consider an arbitrary cross section of a porous material as illustrated in Fig. 2. The pores are randomly oriented and the pressure in the pores acts on an average area $2\pi r_p^2$. The net force due to the pressure in the pores must balance the internal tensile stress σ of the solid portion of the material. Fracture occurs when

$$\int_{r_{\min}}^{r_{\max}} p_G(r_p) 2\pi r_p^2 \bar{g}(r_p)\, \mathrm{d}r_p \ge \sigma_{\max}(1-\theta) \tag{14}$$

Equation (14) describes the conditions for fracture in a plane located distance x_f from the free surface. Since the distance x_f scales with the tree height, integration of Eq. (14) at constant x_f is approximately equivalent to integration at constant ℓ_t. Using Eq. (11) for $p_G(r_p)$, the fracture criterion becomes

$$p_{\max}\theta > \sigma_{\max}(1-\theta)\beta \tag{15}$$

where $p_{\max}$ is the gas pressure in the smallest pores,

$$p_{\max} = \frac{2x_f}{r_{\min}}(k\mu_G p_{\mathrm{ref}})^{1/2} \tag{16}$$

and it has been assumed that $\ell_t = x_f$. Equations (15) and (16) may be combined into the single criterion for fragmentation

$$x_f > \frac{\sigma_{\max}\beta(1-\theta)r_{\min}}{2\sigma(k\mu_G p_{\mathrm{ref}})^{1/2}} \tag{17}$$

Equation (17) simply dictates that if the pyrolysis rate k were maintained at a sufficiently large value at a sufficient depth x_f, the fluid mechanical pressure will be sufficient to exceed the material yield stress $\sigma_{\max}$. The largest value of x_f satisfying Eq. (17) will represent the thickness of the fragmentation zone. However, satisfying Eq. (17) does not insure that the theoretical gas pressure in the pore has not exceeded the limiting value p_{limit}. This case is included by using $p_G = p_{\mathrm{limit}}$ for $r_p < r_{jV}$ and p_G as given by Eq. (12) for $r_p \ge r_{jV}$ in the fragmentation criterion [Eq. (14)]. The fragmentation criterion becomes

$$x_f > \frac{p_{\mathrm{limit}} r_{\min}}{2(k\mu_G p_{\mathrm{ref}})^{1/2}}\left\{\exp\left[\frac{\beta\sigma_{\max}{}^{(1-\theta)}}{\theta p_{\mathrm{limit}}}\right] - 1\right\} \tag{18}$$

which, in the limit of

$$\sigma_{\max} < \frac{\theta p_{\mathrm{limit}}}{\beta(1-\theta)} \tag{19}$$

reduces to Eq. (17).

Equation (18) is a general mathematical criterion for the onset of fragmentation and solid mass removal from a laser-irradiated target due to in-depth pyrolysis. This general criterion is reduced to the simultaneous satisfaction of Eqs. (17) and (19). The target material must be heated to the extent that its yield strength falls below the threshold given by Eq. (19) and then the pyrolysis rate and thermal depth of the heated zone must satisfy Eq. (17). In the analysis that follows, it is assumed that σ_{max} satisfies Eq. (19) and it is necessary to determine only the thermal depth that satisfies Eq. (17).

V. Model Prediction

Consider a laser material interaction which raises the material surface to temperature T and deposits energy over the thermal depth ℓ such that $T(x)$ is given by

$$T(x) = Te^{-x/\ell} \tag{20}$$

where x is measured normal to the surface ($x=0$ at the surface). The pyrolysis rate $k(x)$ is assumed to follow $T(x)$ by

$$k(x) = Ae^{-B/T(x)}$$

Table 1 Characteristic values of parameters

A	$5\times10^{11}\ s^{-1}$	r_{min}	0.2 nm
B	20,000 K	β	10
M	0.1 MPa	$\bar{V}$	10^3 m/s
N	2,000 K	θ_f	0.2
B_0	12,000 K	μ_G	10^{-4} kg/m·s
x_0	0.01 nm	ρ_s	1 g/cm^3

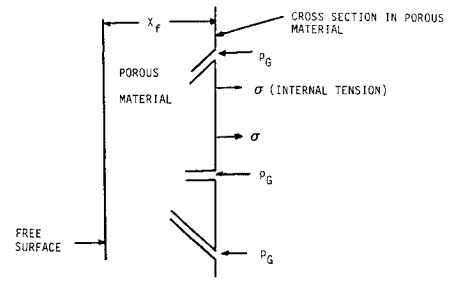

Fig. 2 Particle fragmentation.

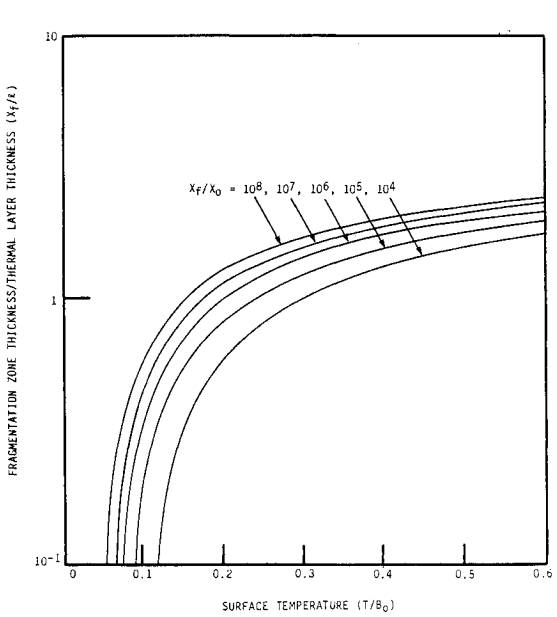

Fig. 3 Fragmentation zone thickness.

where B is the activation energy ($B\approx$ 20,000 K for coal) and A a pre-exponential factor ($A\approx5\times10^{+11}\ s^{-1}$ such that $k=10^3\ s^{-1}$ at 1000 K). The yield stress of the material is assumed to decay with temperature as

$$\sigma_{max}(x) = Me^{N/T(x)}$$

where N is approximately 2000 K and $M\approx0.1$ MPa such that σ_{max} is order 0.1 GPa (1000 atm) at 300 K and decays rapidly at temperatures of order 1000 K, which is characteristic of organic composites.

Eliminating $T(x)$, $k(x)$, and $\sigma_{max}(x)$ from Eq. (17), the fracture condition is now expressed as

$$\frac{x_f}{\ell} = \ln\left[\frac{T}{B_0}\ln\left(\frac{x_f}{x_0}\right)\right] \tag{21}$$

where

$$B_0 = N + \tfrac{1}{2}B$$

$$x_0 = \frac{2M\beta\, r_{min}}{\bar{V}\theta_f(A\mu_G\rho_s)^{1/2}}$$

and it has been assumed that

$$(1-\theta)\Big/\left[\frac{2\pi\theta}{\theta_f}\left(1-\frac{\theta}{\theta_f}\right)\right]^{1/2} \approx 1$$

The fracture criterion [Eq. (17)] was derived for the case of a uniform particle temperature. The use of a spatially dependent temperature profile requires that Eq. (17) be locally valid at each location x. This suggests that the pressure is dominated by the conditions at x and not by the conditions between x and the particle surface ($r_p = r_t$). This hypothesis is supported in the derivation of Eq. (11) for the gas pressure in the pores.

Equation (21) very clearly demonstrates that x_f is of order ℓ! Typical values of these parameters for coals and organic composites are tabulated in Table 1. For values of the thermal depth in the 10 μm range, ℓ/x_0 is of order 10^6 and x_f/ℓ is 1.24 at $T=3000$ K. The sensitivity of x_f/ℓ to ℓ/x_0 and T/B_0 is illustrated in Fig. 3. The thickness of the fragmentation zone is first order in the thermal depth ℓ, logarithmic in surface temperature T and activation energy B_0, but relatively insensitive to all other parameters, provided ℓ/x_0 exceeds 10^2.

Rewriting the temperature profile [Eq. (20)] at $x=x_f$

$$\frac{x_f}{\ell} = \ln\left[\frac{T}{T(x_f)}\right]$$

and comparing to the fracture criterion [Eq. (21)], it is apparent that the temperature at the fracture location is approximately constant,

$$T(x_f) = \frac{B_0}{\ln(x_f/x_0)} \approx \frac{B_0}{\ln(\ell/x_0)} \approx 1000\ \text{K}$$

A constant temperature implies a constant energy density, approximately 1 kJ/g corresponding to 1000 K. While the heat of pyrolysis of many materials does exceed 1 kJ/g, it is noted that only a small fraction of the target need be pyrolyzed. Hence, the heat of pyrolysis represents only a small perturbation to the energetics. However, the rate of pyrolysis may be crucial! The above analysis requires that the temperature rises to 1000 K in a time scale less than the pyrolysis time scale; otherwise, the volatiles will have been released at a relatively slow rate and sufficient internal pressure would not develop. These possibilities are readily incorporated into an analysis of the threshold pulse fluence.

VI. Threshold Pulse Fluence

The fluence F of a single laser pulse refers to the energy per unit area (J/cm^2) either in the laser beam, delivered to the target surface, or that absorbed by the target. Below, pulse fluence refers only to the actual fluence absorbed by the target. The threshold fluence $F_{\rm th}$ is the fluence corresponding to the onset of fragmentation at $x_f=\ell$. The threshold fluence is a function of many target parameters and there will be a minimum threshold fluence $F_{\rm thm}$ that is appropriate to certain regimes in parameter space.

The absorbed fluence F that induces the thermal profile [Eq. (20)] may be expressed as

$$F=\rho_s \ell c T(0)$$

where c is the specific heat of the target material. The threshold pulse fluence is that value of F that induces temperature $B_0/\ell n(\ell/x_0)$ at $x_f=\ell$. This fluence is expressed as

$$F_{\rm th}=\frac{\rho_s \ell c B_0 e}{\ell n(\ell/x_0)} \tag{22}$$

where e is the base of the natural logarithm. Various limits of Eq. (22) are examined below.

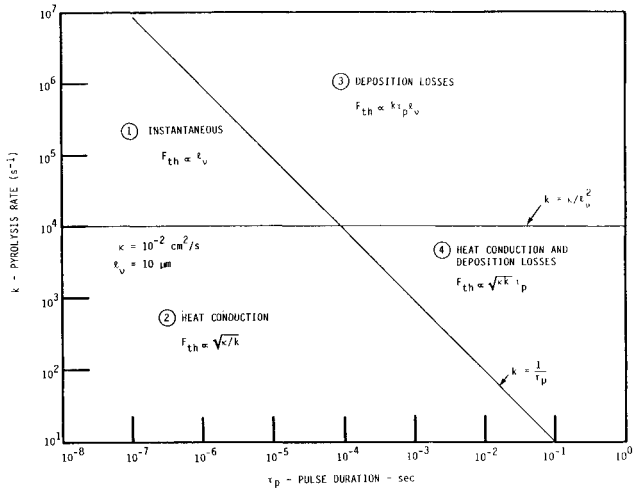

Fig. 4 Threshold pulse fluence scaling regimes.

When a single pulse of energy is irradiated onto a target with absorption depth ℓ_ν, there are three time scales of interest: the laser pulse duration τ_p, the pyrolysis time $1/k$, and the thermal conduction time ℓ_ν^2/κ, where κ is the thermal diffusivity of the target ($\kappa\simeq 10^{-2}$ cm^2/s). If the energy deposition time is fast with respect to pyrolysis and pyrolysis is fast with respect to thermal conduction, there are no losses and Eq. (22) with $\ell=\ell_\nu$ represents the minimum value of the threshold fluence.

Case 1: Instantaneous deposition,

$$\tau_p<1/k<\ell_\nu^2/\kappa$$

$$\ell=\ell_\nu \tag{23}$$

$$F_{\rm thm}=\frac{\rho_s \ell_\nu c B_0 e}{\ell n(\ell_\nu/x_0)} \tag{24}$$

The case of instantaneous deposition corresponds to the highest possible energy density at fluence F because there are no losses. Whenever the thermal conduction time is less than the pyrolysis time, the thermal layer will spread by conduction in the time scale $1/k$. The fragmentation process is pyrolysis limited and the thermal depth ℓ becomes $(\kappa/k)^{1/2}$.

Case 2: Pyrolysis limited,

$$\tau_p<\ell_\nu^2/\kappa<1/k \text{ or } \ell_\nu^2/\kappa<\tau_p<1/k$$

$$\ell=(\kappa/k)^{1/2} \tag{25}$$

$$F_{\rm th}=\frac{\rho_s c B_0 e}{\ell n(\ell/x_0)}\left(\frac{\kappa}{k}\right)^{1/2} \tag{26}$$

When the pyrolysis time scale is short with respect to the pulse duration τ_p, the pyrolysis is over before the entire fluence is absorbed by the target. Thus, only $(k\tau_p)^{-1}$ of the pulse fluence can be utilized for fracture. The process is deposition limited and the threshold pulse fluence must be increased by the factor $k\tau_p$ in order for the target to reach the critical fracture temperature in time $1/k$.

Case 3: Deposition limited,

$$1/k<\ell_\nu^2/\kappa<\tau_p \text{ or } 1/k<\tau_p<\ell_\nu^2/\kappa$$

$$\ell=\ell_\nu \tag{27}$$

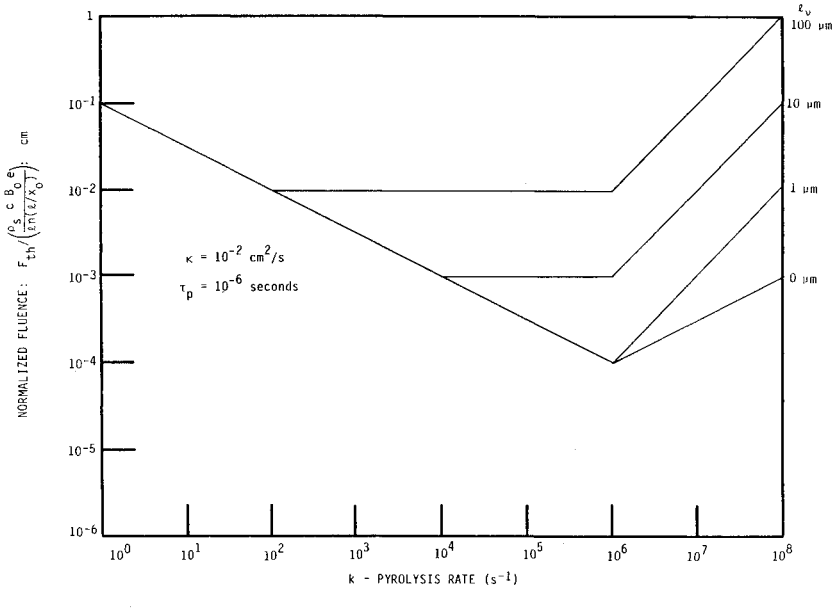

Fig. 5 Threshold pulse fluence.

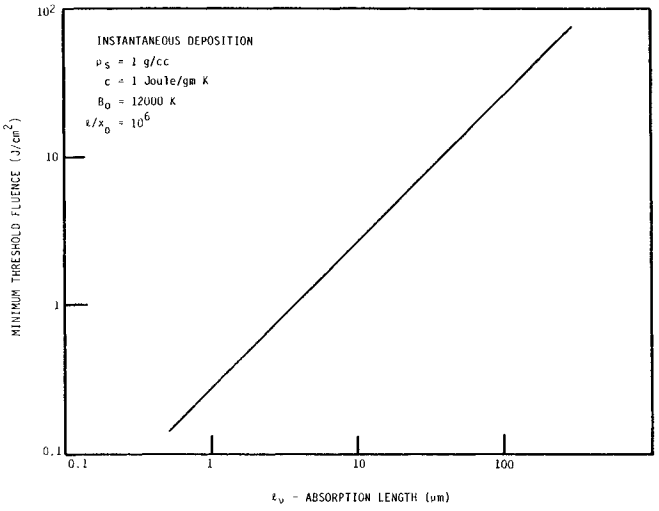

Fig. 6 Minimum threshold pulse fluence.

$$F_{th} = \frac{\rho_s \ell_v c B_0 k \tau_p e}{\ell n(\ell_v/x_0)} \tag{28}$$

Case 4: Deposition limited,

$$\ell_v^2/\kappa < 1/k < \tau_p \qquad \ell = (\kappa/k)^{1/2} \tag{29}$$

$$F_{th} = \frac{\rho_s c B_0 \tau_p e}{\ell n(\ell/x_0)} (\kappa k)^{1/2} \tag{30}$$

The four cases described above are illustrated in Fig. 4 for $\ell_v = 10$ μm and $K = 10^{-2}$ cm^2/s. The threshold pulse fluence is a minimum in region 1, as there are heat conduction losses in region 2, deposition losses in region 3, and both forms of losses in region 4. The fact that the instantaneous deposition region (region 1) does represent a minimum threshold pulse fluence is illustrated in Fig. 5. At low pyrolysis rates, the required fluence is increased by thermal conduction. At high pyrolysis rates, the required fluence is increased due to the completion of the pyrolysis before energy deposition is complete. The minimum fluence lies in region 1. Values of this minimum fluence are illustrated in Fig. 6 as a function of the absorption length ℓ_v. For $\ell_v = 10$ μm, fragmentation and blowoff will occur for an absorbed fluence of 2.5 J/cm^2, provided the pulse duration and pyrolysis rate lie in region 1 of Fig. 4.

VII. Conclusions

A criterion for pyrolysis-induced fragmentation of laser-irradiated surfaces has been developed. It has been expressed in a form that may be used with a computer calculation of in-depth laser absorption. Fragmentation occurs for all x such that

$$x > \frac{p_{limit} r_{min}}{\bar{V}} \left[\frac{2\theta}{\pi k \rho_s \mu_G (\theta_f - \theta)}\right]^{1/2} \left\{\exp\left[\frac{\beta(1-\theta)\sigma_{max}}{\theta p_{limit}}\right] - 1\right\} \tag{31}$$

where x is the distance below the irradiated surface, p_{limit} the maximum gas pressure that can exist in the pores (the pressure corresponding to solid density ρ_s and temperature T), $\beta = \sim 10$, r_{min} is the radius of the smallest pore, σ_{max} the material yield stress, $\bar{V}$ the mean thermal speed of a molecule, k the bulk pyrolysis rate, μ_G the gas viscosity, θ the local porosity, and θ_f the final porosity of the pyrolyzed material.

Idealized thermal profiles (exponential with depth) and pyrolysis rates (Arrhenius) have been used to obtain analytic results for the fragmentation thickness and threshold pulse fluence in terms of the physical parameters of the system. The thickness of the fragmentation zone is approximately the thermal depth at time $1/k$, and is relatively insensitive to all other parameters. The threshold pulse fluence (J/cm^2 absorbed by target) necessary to obtain fragmentation is sensitive to the laser pulse duration, the pyrolysis rate, and the laser absorption depth ℓ_v. A minimum threshold pulse fluence is predicted for short pulse durations, short absorption lengths, and moderate pyrolysis rates. Under optimum conditions, a 10 μm fragmentation zone can be obtained with an absorbed fluence of 2.5 J/cm^2.

Acknowledgment

This work was funded by the U.S. Army Ballistic Missile Defense Advanced Technology Center under Contract DASG60-82-C-0016 through a subcontract with R&D Associates, Marina del Rey, CA.

References

[1]Simons, G.A., "Coal Pyrolysis, I. Pore Evolution Theory," *Combustion and Flame,* Vol. 53, 1983, pp. 83-92.

[2]Simons, G.A., "Coal Pyrolysis, II. Species Transport Theory," *Combustion and Flame,* Vol. 55, 1984, pp. 181-194.

[3]Russell, W.B., Saville, D.A., and Greene, M.I., "A Model for Short Residence Time Hydropyrolysis of Single Coal Particles," *AIChE Journal,* Vol. 25, 1979, pp. 65-80.

[4]Gavalas, G.R. and Wilks, K.A., "Intraparticle Mass Transfer in Coal Pyrolysis," *AIChE Journal,* Vol. 26, 1980, pp. 201-212.

[5]Schneider, P.J., Dolton, T.A., and Reed, G.W., "Mechanical Erosion of Charring Ablators in Ground-Test and Re-Entry Environments," *AIAA Journal,* Vol. 6, 1968, pp. 64-72.

[6]Gavalas, G.R., "A Random Capillary Model with Application to Char Gasification at Chemically Controlled Rates," *AIChE Journal,* Vol. 26, 1980, pp. 577-586.

[7]Gavalas, G.R., "Analysis of Char Combustion Including the Effect of Pore Enlargement," *Combustion Science and Technology,* Vol. 24, 1981, pp. 197-210.

[8]Bhatia, S.K. and Perlmutter, D.D., "A Random Pore Model for Fluid-Solid Reactions: II. Diffusion and Transport Effects," *AIChE Journal,* Vol. 27, 1981, pp. 247-254.

[9]Bhatia, S.K. and Perlmutter, D.D., "The Effect of Pore Structure on Fluid-Solid Reactions: Application to the SO_2-Lime Reaction," *AIChE Journal,* Vol. 27, 1981, pp. 226-234.

[10]Simons, G.A. and Finson, M.L., "The Structure of Coal Char: Part I, Pore Branching," *Combustion Science and Technology,* Vol. 19, 1979, pp. 217-225.

[11]Simons, G.A., "The Strucutre of Coal Char: Part II, Pore Combination," *Combustion Science and Technology*, Vol. 19, 1979, pp. 227-235.

[12]Simons, G.A., "The Pore Tree Structure of Porous Char," *19th Symposium (International) on Combustion,* The Combustion Institute, Pittsburgh, PA, Aug. 1982, pp. 1067-1076.

[13]Simons, G.A., "The Role of Pore Structure in Coal Pyrolysis and Gasification," *Progress in Energy and Combustion Science,* Vol. 9, 1983, pp. 269-290.

[14]Kothandaraman, G. and Simons, G.A., "Evolution of the Pore Structure in PSOC 140 Lignite During Pyrolysis," *20th Symposium (International) on Combustion,* The Combustion Institute, Pittsburgh, PA, 1984, pp. 1523-1529.

[15]Simons, G.A., and Rawlins, W.T., "The Reaction of Sulfur Dioxide and Hydrogen Sulfide with Porous Calcined Limestone," *Industrial Engineering Chemistry, Process, Design and Development,* Vol. 19, 1980, pp. 565-572.

[16]Ham, D., Gelb, A., Lord, G., and Simons, G., "Hot Gas Cleanup for Molten Carbonate Fuel Cells—Dechlorination and Soot Formation," Physical Sciences Inc., Andover, MA, PSI TR-398, Final Tech. Rept., Contract DE-AC21-81MC16242, Jan. 1984.

[17]To be published.